SCIENTIFIC REPORTS

OPEN

SUBJECT AREAS:
NANOPARTICLES
COLLOIDS
POLYMERS
STRUCTURAL PROPERTIES

Received
21 January 2013

Accepted
27 February 2013

Published
12 March 2013

Correspondence and requests for materials should be addressed to D.W. (wudc@mail.sysu.edu.cn)

Highly Monodisperse Microporous Polymeric and Carbonaceous Nanospheres with Multifunctional Properties

Yi Ouyang, Huimin Shi, Ruowen Fu & Dingcai Wu

Materials Science Institute, PCFM Lab and DSAPM Lab, School of Chemistry and Chemical Engineering, Sun Yat-Sen University, Guangzhou 510275, P. R. China.

Fabrication of monodisperse porous polymeric nanospheres with diameters below 500 nm remains a great challenge, due to serious crosslinking between neighboring nanospheres during pore-making process. Here we show how a versatile hypercrosslinking strategy can be used to prepare monodisperse microporous polystyrene nanospheres (MMPNSs) with diameters as low as *ca.* 190 nm. In our approach, an unreactive crosslinked PS outer skin as protective layer can be *in-situ* formed at the very beginning of hypercrosslinking treatment to minimize the undesired inter-sphere crosslinking. The as-prepared MMPNSs with a well-developed microporous network demonstrate unusual multifunctional properties, including remarkable colloidal stability in aqueous solution, good adsorption-release property for drug, and large adsorption capacity toward organic vapors. Surprisingly, MMPNSs can be directly transformed into high-surface-area monodisperse carbon nanospheres with good colloidal stability via a facile hydrothermal-assisted carbonization procedure. These findings provide a new benchmark for fabricating well-defined porous nanospheres with great promise for various applications.

Monodisperse porous nanospheres benefit from the remarkable and complementary property of well-developed porous porosity and zero-dimensional (0D) nanoscale morphology. Their well-defined porous structure, large surface area and unique nanospherical shape make porous nanospheres quite useful in adsorption[1], drug delivery[2–5], energy storage[6,7], and catalysis[8–12]. Many monodisperse porous inorganic nanospheres, such as silicate[4,5,9,13–18] and metal (oxides)[6,12,19–25] have been extensively synthesized based on sol-gel chemistry[24,26], solvothermal chemistry[27], and template method[28,29]. However, their organic counterparts, i.e., monodisperse porous polymeric nanospheres, have attracted much less attention, although they have unique advantages, including facile incorporation of multiple chemical funtionalites, and weight advantage because of composition of light elements[30].

Up to now, it remains a great challenge to fabricate monodisperse porous polymeric nanospheres with diameter below 500 nm, considering that most of them always demonstrate poor polydispersity[31,32] or have much larger particle sizes[33,34]. This could be because during normal crosslinking treatment for introduction of pore structure into nanosphere, the undesired crosslinking between neighboring nanospheres will be inevitable when the particle size is below 500 nm and will become more and more serious with further decreasing the particle size. To avoid the inter-sphere crosslinking phenomenon, researchers have developed a "protective crosslinking" strategy[35]. Nevertheless, this method is somewhat complex and costly given its multiple synthetic steps and sacrificial use of protective block copolymer outer shell.

Herein we describe the synthesis of highly monodisperse microporous polystyrene (PS) nanospheres (MMPNSs) with diameters as low as 190 nm based on a facile hypercrosslinking strategy. As shown in Figures 1 and S1, monodisperse PS nanospheres with divinylbenzene precrosslinking were initially prepared as the precursor, and subsequently were treated with a simple hypercrosslinking procedure to obtain the monodisperse microporous PS nanospheres. The fast hypercrosslinking of the PS chains on the periphery of PS nanospheres leads to the rapid formation of almost unreactive crosslinked PS outer skin and thus minimizes the undesired inter-sphere crosslinking, providing a high monodispersity to the product. The intra-sphere

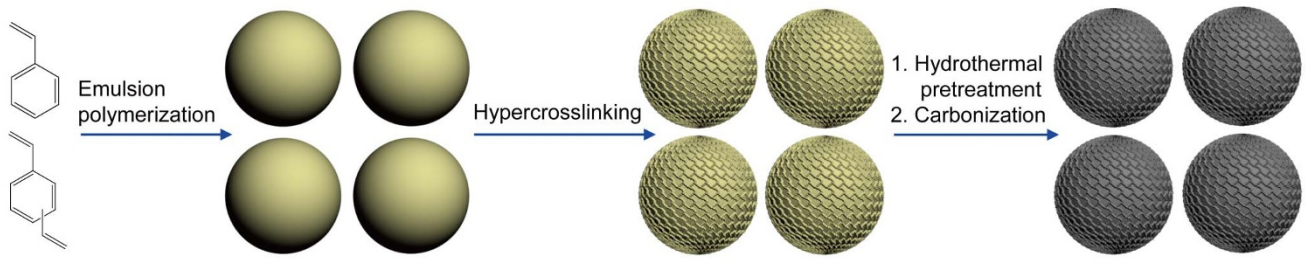

Figure 1 | Illustration for preparation of monodisperse microporous polymeric and carbonaceous nanospheres.

hypercrosslinking creates a well-developed microporous network inside a single PS nanosphere. This method reveals a highly versatile approach for preparation of monodisperse porous polymeric nanospheres.

The as-prepared MMPNSs with high surface areas demonstrate multifunctional properties, including remarkable colloidal stability in aqueous solution, good adsorption-release performance of drugs, and high adsorption capacity toward organic vapors. To the best of our knowledge, such small-sized MMPNSs with highly desired multifunctionality have not been reported yet. Furthermore, we discovered that MMPNSs of this type can be successfully transformed into monodisperse microporous carbon nanospheres (MMCNSs) via a unique hydrothermal-assisted carbonization procedure. Such a reliable procedure represents a great advance for fabrication of carbonaceous nanospheres from polymeric counterparts without sacrificing the desired monodispersibility during pyrolysis. We hope that the as-prepared MMPNSs and MMCNSs can find use in a spectrum of potential applications, including air cleaning, drug delivery and energy storage.

Results

The typical monodisperse PS nanosphere sample PS-1 presented a very low polydispersity index (PDI) of 0.005, as measured by dynamic light scattering (DLS), Figure S2a, and demonstrated perfect spherical morphology, according to SEM image in Figure S2b. The diameter of PS-1 was measured to be 228 nm by means of SEM image analysis, Figure S2c. PS-1 was subsequently treated with a simple hypercrosslinking procedure based on Friedel-Crafts reaction of PS chains with the crosslinker carbon tetrachloride (CCl_4) to produce a MMPNS sample MMPNS-CT1. We found that upon addition of catalyst anhydrous aluminum chloride, the color of PS nanosphere solution in CCl_4 at 75°C was changed quickly from milky to brick-red after 1 minute and to black after 2 minutes (Figure S3a), revealing a very fast hypercrosslinking rate. At the very beginning, the hypercrosslinking reaction only occurred on the periphery of PS nanospheres, since the catalyst initially existed around PS nanospheres. This led to the rapid formation of an almost unreactive crosslinked outer skin for each PS nanosphere, thus minimizing the undesired crosslinking reaction between neighboring PS nanospheres. After that, the catalyst gradually penetrated through the outer skin into the inside to undergo the intra-sphere hypercrosslinking, leading to the product MMPNS-CT1. The MMPNS-CT1 had a weight gain of about 28 wt.% because of the introduction of –CO– crosslinking bridges from the crosslinker CCl_4 (Figures S5 and S6)[36–39], which could be translated into the molar ratio of styrene unit to –CO– bridge approximately equal to 1, indicating a hypercrosslinked structure characteristic.

DLS curve in Figure 2a clearly shows that the as-prepared MMPNS-CT1 demonstrated very high monodispersity characteristic with a PDI of 0.005, which is supported by SEM image in Figure 2b and TEM image in Figure 2c. The diameter of MMPNS-CT1 was measured to be 246 nm, according to the SEM image analysis, Figures 2b and S7a. In order to prove the importance of rapid hypercrosslinking for such high monodispersity, a control experiment was carried out at a low reaction temperature (i.e., 0°C) to slow down the hypercrosslinking rate (Figure S3b). Just as expected, the resulting control sample had a much larger hydrodynamic diameter (473 *vs* 228 nm) and a much higher PDI (0.105 *vs* 0.005) than its precursory PS-1 (Figure S4), indicative of obvious crosslinking between nanospheres in the case of slow hypercrosslinking reaction. High-resolution TEM image in Figure 2d reveals that MMPNS-CT1 presented a unique 3D network-type microporosity, because of its hypercrosslinked structure characteristic (Figure S5)[37–39]. The introduction of microporosity is well supported by a slight increase of particle diameter for MMPNS-CT1 relative to its precursory PS-1 (246 *vs* 228 nm), Figure S7a. Furthermore, such a micropore structure can also be confirmed by an obvious adsorption uptake at low relative pressure in the N_2 adsorption-desorption isotherm of Figure 3a. According to the pore size distribution curve by density functional theory (DFT)[40,41] in Figure 3b, micropores of MMPNS-CT1 were centered at 0.7 and 1.3 nm in diameter. A Brunauer-Emmett-Teller (BET) calculation gave the BET surface area (S_{BET}) for MMPNS-CT1 equal to 386 m^2g^{-1}, and the total pore volume (V_t) was calculated to be 0.28 cm^3g^{-1} according to the amount adsorbed

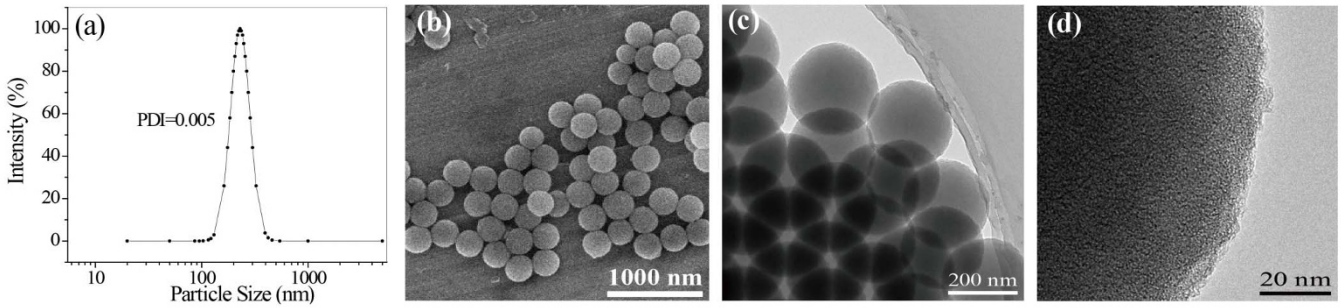

Figure 2 | DLS curve (a), SEM image (b), TEM image (c) and high-resolution TEM image (d) of the representative monodisperse microporous polymeric nanosphere sample MMPNS-CT1 obtained by hypercrosslinking of PS-1.

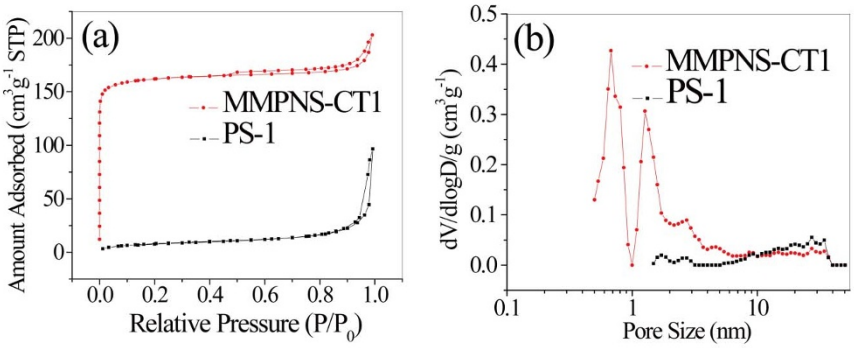

Figure 3 | N_2 adsorption-desorption isotherm (a) and DFT pore size distribution curve (b) for PS-1 and MMPNS-CT1.

at a relative pressure P/P_0 of *ca.* 0.99. In contrast, its precursory PS-1 without hypercrosslinking treatment did not have micropores (Figure 3), thus demonstrating the S_{BET} and V_t as low as 30 m^2g^{-1} and 0.15 cm^3g^{-1}, respectively.

In order to test the universality of the hypercrosslinking strategy, we replaced the above crosslinker CCl_4 with other crosslinkers such as formaldehyde dimethyl acetal (FDA) and divinylbenzene (DVB) to treat PS-1. As shown in Figure 4 and Figure S7, the as-obtained MMPNS samples, i.e., MMPNS-FDA with $-CH_2-$ crosslinking bridges and MMPNS-DVB with $-(CH_3)CHC_6H_4CH(CH_3)-$ crosslinking bridges (Figure S5), still presented almost the same DLS curves and SEM images as the MMPNS-CT1, indicating that the inter-sphere crosslinking was also avoided successfully in these two hypercrosslinking systems. Likewise, due to the introduction of micropore structure (Figure S8), MMPNS-FDA and MMPNS-DVB had high S_{BET} equal to 527 and 332 m^2g^{-1}, respectively, and had large V_t of 0.35 and 0.24 cm^3g^{-1}, respectively.

Furthermore, we demonstrated that the hypercrosslinking approach was still feasible for fabricating MMPNSs with smaller diameters. When decreasing the diameter of PS nanospheres from *ca.* 330 to *ca.*170 nm (Figures S9 and S10), the resulting MMPNS-CT3 with diameter of about 190 nm (Figure S10d) still had good monodispersity with a low PDI of 0.05 (Figure 5c). The S_{BET} and V_t of MMPNS-CT3 were measured to be 407 m^2g^{-1} and 0.42 cm^3g^{-1}, respectively. However, when the hydrodynamic diameter of PS nanospheres was further decreased to 58 nm (Figure S9c), the corresponding crosslinked product CPS presented much higher hydrodynamic diameter and PDI (1273 *vs* 58 nm and 0.294 *vs* 0.012, respectively), Figure S9d. This is because such small nanospheres had a much higher collision probability in solution arising from much higher surface area, and then led to severe crosslinking between neighboring nanospheres.

To demonstrate usefulness and advantage of the unique MMPNSs, we studied their colloidal stability, adsorption properties and carbonization performance. It is known that crosslinked polymeric nanospheres often cannot be dispersed in aqueous solution because of lack of colloidal stability[42,43]. Surprisingly, we found that MMPNSs, e.g., MMPNS-CT1, can be directly dispersed in water, and the obtained buff colloidal dispersion of MMPNS-CT1 was well stable, judging from the fact that no any precipitation occurred after standing for a long time, e.g., 30 days, Figure 6a. In contrast, CPS with severe inter-sphere crosslinking failed to stably disperse in water (Figure S11). Such a good colloidal stability of MMPNSs can be well supported by Zeta potential measurement. Figure 6b gives Zeta potentials of MMPNS-CT1 dispersion in aqueous solution with different pH values. It can be clearly seen that over the total pH range from 2 to 13, its Zeta potentials were basically below −30 mV. This indicates that the sphere surface of MMPNS-CT1 was negatively charged, which could be derived from the potassium persulfate initiator for emulsion polymerization (Figure S12). More importantly, the absolute value of above 30 mV confirms that MMPNS-CT1 can be stably dispersed in aqueous solution, because of strong electrostatic repulsion.

It is known that aggregation and ununiformity of drug carriers often lead to an inferior targeting, reducing the efficiency of therapeutic drug[44]. Obviously, this class of discrete and uniform MMPNSs with good dispersibility in aqueous solution should have a great potential for use as drug carriers. Thus, we characterized the adsorption and release performance of drug model captopril for MMPNS-CT1 in aqueous solution at body temperature (37°C). We found that MMPNS-CT1 showed a high adsorption capacity toward captopril, i.e., 100 mg g^{-1}, a quite substantial value. More importantly, MMPNS-CT1 was found to have no obvious initial burst release, which helps reduce many side effects[45]. For example, in the first 1h, only 5 wt.% of captopril was released (Figure 7a), which was negligible. After 48 h, 58 wt.% of drug was released, indicating a good sustained-release behavior. In addition, it was found that the reused MMPNS-CT1 still released 51 wt.% of captopril at 48 h (Figure 7a), demonstrating good recycling performance.

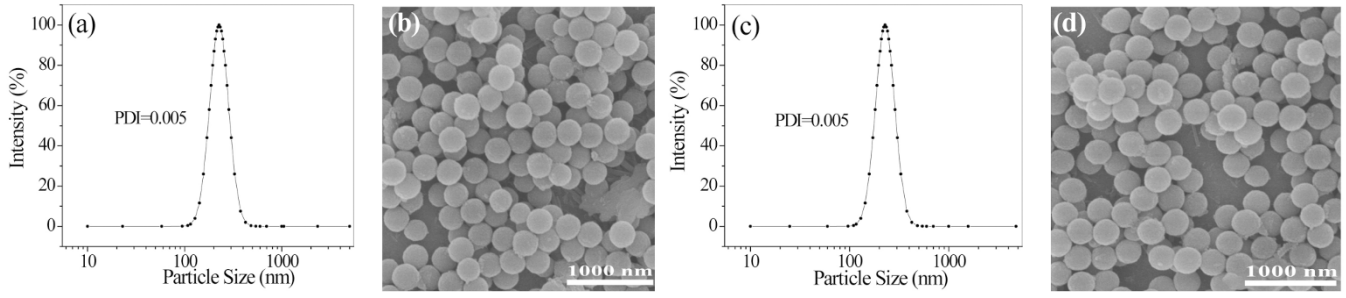

Figure 4 | DLS curve (a) and SEM image (b) of MMPNS-FDA; and DLS curve (c) and SEM image (d) of MMPNS-DVB.

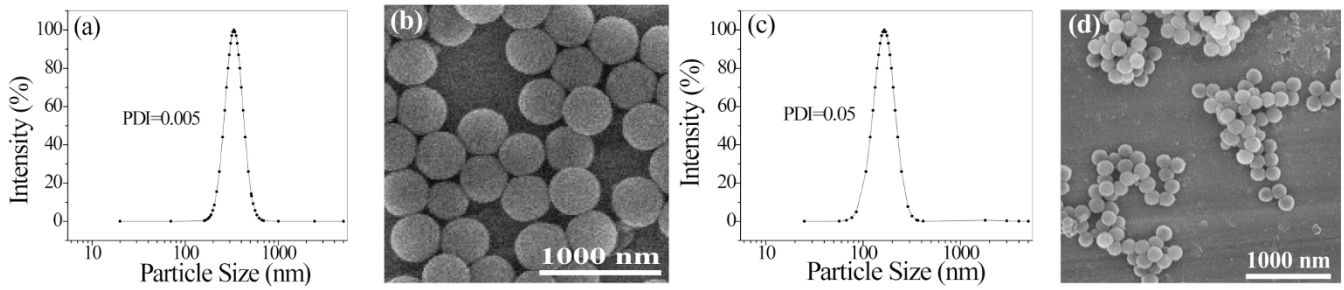

Figure 5 | DLS curve (a) and SEM image (b) of MMPNS-CT2; and DLS curve (c) and SEM image (d) of MMPNS-CT3.

Besides the above adsorption properties toward drugs, we also explored the adsorption performance toward organic vapors for MMPNSs. It can be found from Figure 7b that MMPNS-CT1 has high adsorption capacities toward organic vapors such as toluene and methanol at various relative pressures. For example, at P/P_0 = 0.9, the specific adsorption capacity per unit surface area for MMPNS-CT1 was 0.91 and 0.93 mg m^{-2} for methanol and toluene, respectively, which was comparable to that of ordered mesoporous polymer[38].

Generally, carbonization is an important approach to provide novel structures and properties to polymer-based materials, such as achieving conductive and electrochemical performances[46–51] and generating micropores[52–54], which greatly extends their applications. Therefore, we tried to produce MMCNSs by carbonization of MMPNSs. We found that direct carbonization of MMPNS-CT1 at 900°C failed to obtain monodisperse carbonized product, because of very serious particle agglomeration which commonly occurs during high-temperature pyrolysis for carbon materials (Figures S13 and S14). However, we surprisingly discovered that when imposing a simple hydrothermal pretreatment at 180°C on MMPNS-CT1 (Figure S15), a well-defined discrete MMCNS product with a carbonization yield of 38 wt.% can be successfully fabricated by subsequent pyrolysis at 900°C. MMCNS presented a very low PDI of 0.005 (DLS curve in Figure 8a) and a perfect spherical morphology (TEM image in Figure 8b). The diameter of MMCNS was measured to be 224 nm by analyzing SEM image (Figure S15c), which was smaller than that of MMPNS-CT1 (246 nm), indicating a framework shrinkage because of mass loss after carbonization. The graphitic crystallite structure of MMCNS was investigated by Raman spectroscopy (Figure S16). The Raman spectrum with a Gauss Fit Multipeaks analysis showed that MMCNS had four bands around 1170, 1345, 1539, and 1600 cm^{-1}. The band around 1600 cm^{-1}, known as the G (graphitic) mode, was attributed to "in-plane" zone-center atomic vibrations of large graphite crystallites[55]. The band around 1345 cm^{-1}, often called as D (disordered) mode, was ascribed to the phonons near the Brillouin zone boundary active in small crystallites or on the boundaries of larger crystallites[56]. In addition, there were two weak bands around 1100 and 1530 cm^{-1}, denoted as sp^3 and A (amorphous) mode, respectively. The sp^3 mode was attributed to the Raman scattering of sp^3 carbon atoms, indicating low graphite character[57], while the A mode was associated with amorphous sp^2-bonded forms of carbon arising from interstitial defects of MMCNS[58].

As demonstrated in Figure S14b, MMCNS can be well dispersed to water, forming a well stable colloidal dispersion. We revealed that the hydrothermal pretreatment played a role of liquid-phase preoxidation (Figure S17), as evidenced by an obvious increase of oxygen content (18.6 *vs* 16.0%) in Table S1 and appearance of additional carboxylic group in XPS spectrum, Figure S18. This greatly improved the thermal stability of MMPNS-CT1 during carbonization (see TG curves in Figure S19), minimizing the side effect of particle agglomeration. N_2 adsorption measurement showed that as compared to MMPNS-CT1, MMCNS had a significantly higher S_{BET} (1357 *vs* 386 m^2g^{-1}) and a much larger V_t (1.02 *vs* 0.28 cm^3g^{-1}), because of generation of numerous new micropores during pyrolysis (Figures 8c and 8d). The hydrothermal pretreatment was found to facilitate formation of such pyrolysis-induced micropores, as indicated by an obvious increase in S_{BET} (1357 *vs* 542 m^2g^{-1}) and V_t (1.02 *vs* 0.31 cm^3g^{-1}) when comparing carbonized products with and without this pretreatment. To the best of knowledge, there have been rare reports about fabrication of such monodisperse high-surface-area carbon nanospheres without any additional activation posttreatment.

Discussion

We have demonstrated a simple yet versatile approach for the fabrication of discrete, uniform and dispersible MMPNSs based on a hypercrosslinking procedure. The rapid formation of an unreactive crosslinked outer skin at the very beginning of Friedel-Crafts reactions of PS nanospheres can minimize the undesired inter-sphere crosslinking, thus producing individual polymeric nanospheres with a well-developed microporosity. The as-prepared MMPNSs with high surface areas (332–527 m^2g^{-1}) and large pore volumes (0.24–0.42 cm^3g^{-1}) presented remarkable colloidal stability in aqueous

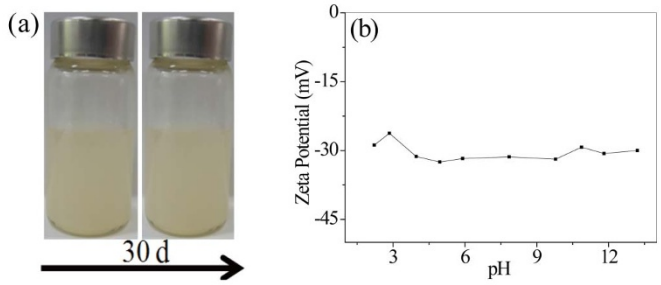

Figure 6 | (a) Photographs of the MMPNS-CT1 dispersion in water before and after standing for 30 days; (b) Zeta potential as a function of pH for the aqueous dispersion of MMPNS-CT1.

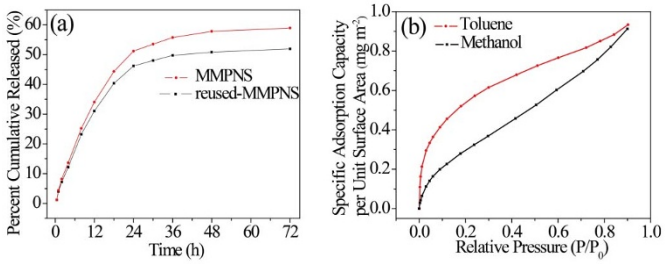

Figure 7 | (a) Cargo release profile of MMPNS-CT1 and reused MMPNS-CT1; (b) specific adsorption capacity toward methanol vapor and toluene vapor at various relative pressures for MMPNS-CT1.

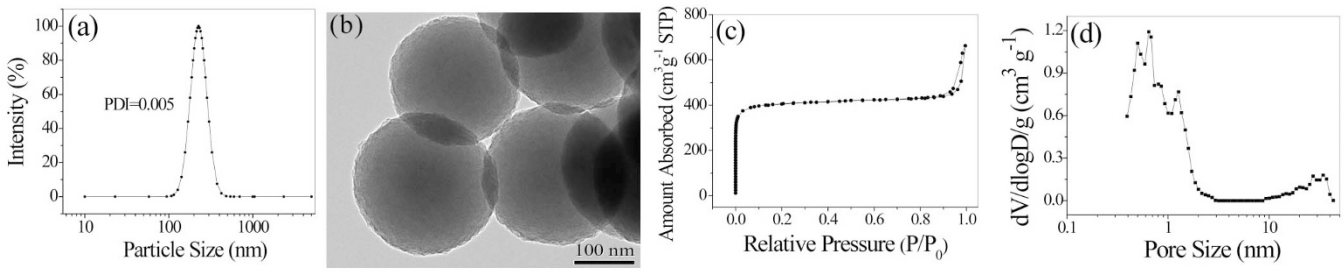

Figure 8 | DLS curve (a), TEM image (b), N_2 adsorption-desorption isotherm (c) and DFT pore size distribution curve (d) for the representative monodisperse microporous carbonaceous nanosphere sample MMCNS obtained by hydrothermal-assisted carbonization of MMPNS-CT1.

solution. MMPNSs were found to perform well as a sustained-release drug carrier with a high drug loading capacity and negligible initial burst release, and as an adsorbent for organic vapors. Furthermore, we discovered that MMPNSs can be extensible to MMCNSs, whose surface area and pore volume were as high as 1357 m^2g^{-1} and 1.02 cm^3g^{-1}, respectively, via a facile hydrothermal-assisted carbonization procedure. To the best of our knowledge, there have been rare reports about the direct transformation from polymeric to carbonaceous framework for small-sized nanospheres without sacrificing the highly desired monodispersibility during carbonization. We hope that these highly monodisperse polymeric and carbonaceous nanospheres with a well-developed microporous network may lead to the discovery of more unique and unusual functions, and thus provide new opportunities for fields such as adsorption, separation, medicine, catalysis and energy.

Methods

Materials. Styrene (St, Aldrich, 99%) was purified by passing through a basic alumina column. Dichloroethane was used after distillation. Divinylbenzene (DVB, Aldrich, 80%), anhydrous aluminum chloride ($AlCl_3$, Aldrich, 99.99%), anhydrous ferric chloride ($FeCl_3$, Aladin, 98%), formaldehyde dimethyl acetal (FDA, Sigma, 98%), carbon tetrachloride (CCl_4, Aldrich, 99.5%), sodium dodecyl sulfate (SDS, Tianjin Chemical Reagent Factory, A.R.) and potassium persulfate (KPS, Tianjin Chemical Reagent Factory, A.R.) were used as received.

Preparation of monodisperse polystyrene (PS) nanospheres with DVB precrosslinking. Monodisperse PS nanospheres were prepared according to the reported literature[59]. PS-1 was synthesized according to the ratio of Water/St/DVB/SDS/KPS =100 ml/2.5 ml/0.5 ml/25 mg/100 mg. SDS was dissolved in deionized water in a three-necked flask. After mechanical stirring for 15 min, the flask was purged with nitrogen. Subsequently, St and half of the total amount of DVB were added. After stirring for another 5 min, KPS was added to initiate the polymerization at 75°C. After 3 h, the rest of DVB was added into the emulsion, and the polymerization was continued for another 24 h. The product was washed in ethanol via three centrifugation/redispersion cycles and then dried at 50°C under vacuum.

Synthesis procedures of PS-2, PS-3 and PS-4 were the same as that of PS-1 except that the amount of SDS was 0 mg, 50 mg and 100 mg, respectively.

Preparation of MMPNSs. For synthesis of MMPNS-CT1, 1.0 g of PS-1 was dispersed and swelled in 30 mL of CCl_4, and then 2.8 g of $AlCl_3$ in 30 ml of CCl_4 was added to the above mixture. The reaction was carried out at 75°C for 24 h under stirring. 50 ml HCl/acetone was added slowly to the resulting mixture. The product was filtered off, washed with acetone, 1 M hydrochloric acid and pure water, and then dried under vacuum.

For preparation of MMPNS-FDA, 0.25 g of PS-1 was dispersed in 40 ml dichloroethane, followed by addition of 2 ml of FDA. After stirring for 15 min, 3 g of $FeCl_3$ was added to the above mixture. The reaction was carried out at 80°C for 24 h under stirring. 50 ml HCl/acetone was added slowly to the resulting mixture. The product was filtered off, washed with acetone, 1 M hydrochloric acid and pure water, and then dried under vacuum.

Preparation procedure of MMPNS-DVB was the same as that of MMPNS-FDA except that DVB was employed as the crosslinker. Preparation procedures of other MMPNSs (i.e., MMPNS-CT2 and MMPNS-CT3) and the control sample CPS were the same as that of MMPNS-CT1 except that PS-2, PS-3 and PS-4 were employed as the raw material, respectively.

Preparation of MMCNS. 0.3 g of MMPNS-CT1 was dispersed in 50 mL of deionized water in a sealed autoclave. Subsequently, the sealed autoclave was kept in 180°C for 5 h. After filtration and drying under vacuum at 50°C, the hydrothermal-pretreated MMPNS-CT1 was carbonized by heating to 900°C with a heating rate of 5°C/min for 3 h under N_2 flow. For comparison, a carbonized product of MMPNS-CT1 without hydrothermal pretreatment was also prepared under the same carbonization condition.

Characterization. Dynamic light scattering (DLS) measurements were carried out at 25°C on a Brookheaven Zeta PALS Instrument with a 532 nm laser at a scattering angle of 90°, providing the PDI and hydrodynamic diameter (i.e., the maximum in the DLS particle size distribution curve). The zeta-potential measurement was conducted on a Brookenheaven Zeta PALS with BI-ZTU titration unit at various pH values and a conductance of 300 μS. The nanostructures of the samples were also investigated by a Hitachi S-3400 scanning electron microscope (SEM), and FEI Tecnai G2 Spirit transmission electron microscope (TEM). About 100 nanospheres in a SEM image were picked at random, and then a statistical analysis of the particle size distribution was carried out. The maximum in the resulting particle size distribution curve was referred to as the diameter of nanospheres. N_2 adsorption measurement was carried out using a Micromeritics ASAP 2012 analyzer at 77 K. The BET surface area (S_{BET}) was determined by Brunauer-Emmett-Teller (BET) theory. The total pore volume (V_t) was estimated from the amount adsorbed at a relative pressure P/P_0 of *ca.* 0.99. The pore size distribution was analyzed by original density functional theory (DFT) combined with non-negative regularization and medium smoothing. The thermal stability of the samples was monitored using a thermogravimetric analysis (TGA Q50) from 80 to 800°C under nitrogen with a heating rate of 10°C/min. FTIR spectrum was collected at room temperature on a Bruker Equinox 55 Fourier transform infrared spectroscopy. The elemental analysis was executed by using the Elemental Analyzer Vario EL. X-ray photoelectron spectroscopy (XPS) (ESCALab250) was used for XPS spectrum, and Raman spectrum was conducted on a Renishaw inVia Laser Micro-Raman Spectrometer. A Hiden IG-3 intelligent gravimetric analyzer was used to determine its adsorption capacity toward organic vapors. Shimadzu UV-Vis-NIR Spectrophotometer was used to detect the adsorption capacity and release profile toward captopril. Captopril loading was performed by immersing the MMPNS samples in an aqueous solution containing 1 mg/ml captopril with stirring at room temperature for 24 h. The adsorption capacity was calculated by measuring captopril concentrations before and after adsorbed by MMPNSs. The release experiment was conducted by putting the captopril-loaded MMPNSs into dialysis bags (molecular weight cut off = 7000), followed by soaking the dialysis bags into distilled water at room temperature. At predetermined time intervals, 1 ml of solution have been taken out to test the amount of released captopril and an equal volume of deionized water was immediately added to keep the volume constant.

1. Zhou, J. B. *et al.* Rattle-type carbon-alumina core-shell spheres: synthesis and application for adsorption for organic dyes. *ACS Appl. Mater. Interfaces* **4**, 2174–2179 (2012).
2. Slowing, I. I., Trewyn, B. G., Giri, S. & Lin, V. S. Y. Mesoporous silica nanoparticles for drug delivery and biosensing applications. *Adv. Funct. Mater.* **17**, 1225–1236 (2007).
3. Lai, C. Y. *et al.* A mesoporous silica nanosphere-based carrier system with chemically removable CdS nanoparticle caps for stimuli-responsive controlled release of neurotransmitters and drug molecules. *J. Am. Chem. Soc.* **125**, 4451–4459 (2003).
4. Liu, J., Qiao, S. Z., Hartono, S. B. & Lu, G. Q. Monodisperse yolk-shell nanoparticles with a hierarchical porous structure for delivery vehicles and nanoreactors. *Angew. Chem. Int. Ed.* **49**, 4981–4985 (2010).
5. Kim, J. *et al.* Multifunctional uniform nanoparticles composed of a magnetite nanocrystal core and a mesoporous silica shell for magnetic resonance and fluorescence imaging and for drug delivery. *Angew. Chem. Int. Ed.* **47**, 8438–8441 (2008).
6. Li, N. *et al.* Battery performance and photocatalytic activity of mesoporous anatase TiO_2 nanospheres/graphene composites by template-free self-assembly. *Adv. Funct. Mater.* **21**, 1717–1722 (2011).
7. Yang, S. B. *et al.* Nanographene-constructed hollow carbon spheres and their favorable electroactivity with respect to lithium storage. *Adv. Mater.* **22**, 838–842 (2010).

8. Huh, S., Chen, H. T., Wiench, J. W., Pruski, M. & Lin, V. S. Y. Controlling the selectivity of competitive nitroaldol condensation by using a bifunctionalized mesoporous silica nanosphere-based catalytic system. *J. Am. Chem. Soc.* **126**, 1010–1011 (2004).
9. Huh, S., Chen, H. T., Wiench, J. W., Pruski, M. & Lin, V. S. Y. Cooperative catalysis by general acid and base bifunctionalized mesoporous silica nanospheres. *Angew. Chem. Int. Ed.* **44**, 1826–1830 (2005).
10. Bradley, C. A., Yuhas, B. D., McMurdo, M. J. & Tilley, T. D. Functionalized silicone nanospheres: synthesis, transition metal immobilization, and catalytic applications. *Chem. Mater.* **21**, 174–185 (2009).
11. Mihalcik, D. J. & Lin, W. Mesoporous silica nanosphere supported ruthenium catalysts for asymmetric hydrogenation. *Angew. Chem., Int. Ed.* **47**, 6229–6232 (2008).
12. Wang, F. *et al.* Porous single-crystalline palladium nanoparticles with high catalytic activities. *Angew. Chem. Int. Ed.* **51**, 4872–4876 (2012).
13. Jiang, X. *et al.* Aerosol-assisted synthesis of monodisperse single-crystalline α-cristobalite nanospheres. *Chem. Commun.* **48**, 1293–1295 (2012).
14. Sumper, M., Lorenz, S. & Brunner, E. Biomimetic control of size in the polyamine-directed formation of silica nanospheres. *Angew. Chem. Int. Ed.* **42**, 5192–5195 (2003).
15. Polshettiwar, V., Cha, D., Zhang, X. & Basset, J. M. High-surface-area silica nanospheres (KCC-1) with a fibrous morphology. *Angew. Chem. Int. Ed.* **49**, 9652–9656 (2010).
16. Huang, X. D., Zhou, L., Yu, C. Z. & Zhao, D. Y. Self-assembly of monodispersed silica nano-spheres with a closed-pore mesostructure. *J. Mater. Chem.* **22**, 11523–11528 (2012).
17. Wei, J. *et al.* Solvent evaporation induced aggregating assembly approach to three-dimensional ordered mesoporous silica with ultralarge accessible mesopores. *J. Am. Chem. Soc.* **133**, 20369–20377 (2011).
18. Deng, X. *et al.* Transparent, thermally stable and mechanically robust superhydrophobic surfaces made from porous silica capsules. *Adv. Mater.* **23**, 2962–2965 (2011).
19. Zhang, F., Shi, Y. F., Sun, X. H., Zhao, D. Y. & Stucky, G. D. Formation of hollow upconversion rare-earth fluoride nanospheres: nanoscale kirkendall effect during ion exchange. *Chem. Mater.* **21**, 5237–5243 (2009).
20. Li, Y. X. *et al.* Hierarchical ZnS-In_2S_3-CuS nanospheres with nanoporous structure: facile synthesis, growth mechanism, and excellent photocatalytic activity. *Adv. Funct. Mater.* **20**, 3390–3398 (2010).
21. Sayle, D. C. *et al.* "Simulating synthesis": ceria nanosphere self-assembly into nanorods and framework architectures. *J. Am. Chem. Soc.* **129**, 7924–7935 (2007).
22. Xiao, M. D., Zhao, C. M., Chen, H. J., Yang, B. C. & Wang, J. F. "Ship-in-a-bottle" growth of noble metal nanostructures. *Adv. Funct. Mater.* **22**, 4526–4532 (2012).
23. Meffre, A. *et al.* A simple chemical route toward monodisperse ironcarbide nanoparticles displaying tunable magnetic and unprecedented hyperthermia properties. *Nano Lett.* **12**, 4722–4728 (2012).
24. Deng, Y. H., Qi, D. W., Deng, C. H., Zhang, X. M. & Zhao, D. Y. Superparamagnetic high-magnetization microspheres with an Fe_3O_4@SiO_2 core and perpendicularly aligned mesoporous SiO_2 shell for removal of microcystins. *J. Am. Chem. Soc.* **130**, 28–29 (2008).
25. Kim, T. *et al.* Mesoporous silica-coated hollow manganese oxide nanoparticles as positive T-1 contrast agents for labeling and MRI tracking of adipose-derived mesenchyrnal stem cells. *J. Am. Chem. Soc.* **133**, 2955–2961 (2011).
26. Liu, J. *et al.* Extension of the stöber method to the preparation of monodisperse resorcinol-formaldehyde resin polymer and carbon spheres. *Angew. Chem. Int. Ed.* **50**, 5947–5951 (2011).
27. Lu, A. H. *et al.* Easy synthesis of hollow polymer, carbon, and graphitized microspheres. *Angew. Chem. Int. Ed.* **49**, 1615–1618 (2010).
28. Schmidt, H. T. & Ostafin, A. E. Liposome directed growth of calcium phosphate nanoshells. *Adv. Mater.* **14**, 532–535 (2002).
29. Yoon, S. B. *et al.* Fabrication of carbon capsules with hollow macroporous core/mesoporous shell structures. *Adv. Mater.* **14**, 19–21 (2002).
30. Rzayev, J. & Hillmyer, M. A. Nanoporous polystyrene containing hydrophilic pores from an ABC triblock copolymer precursor. *Macromolecules* **38**, 3–5 (2005).
31. Sun, G. *et al.* Benzaldehyde-functionalized polymer vesicles. *ACS Nano* **3**, 673–681 (2009).
32. Andrew, G., Liu, G. J. & Tao, J. Star polymers and nanospheres from cross-linkable diblock copolymers. *Macromolecules* **29**, 2487–2493 (1996).
33. Macintyre, F. S., Sherrington, D. C. & Tetley, L. Synthesis of ultrahigh surface area monodisperse porous polymer nanospheres. *Macromolecules* **39**, 5381–5384 (2006).
34. Liu, Q. Q. Monodisperse polystyrene nanospheres with ultrahigh surface area: application for hydrogen storage. *Macromol. Chem. Physic.* **211**, 1012–1017 (2010).
35. Fu, G. D., Shang, Z. H., Liang, H., Kang, E. T. & Neoh, K. G. Preparation of cross-linked polystyrene hollow nanospheres via surface-initiated atom transfer radical polymerization. *Macromolecules* **38**, 7867–7871 (2005).
36. Zeng, Q. C. *et al.* Template-free fabrication of hierarchical porous carbon based on intra-/inter-sphere crosslinking of monodisperse styrene-divinylbenzene copolymer nanospheres. *Chem. Commun.* **46**, 5927–5929 (2010).
37. Wu, D. C. *et al.* Nanoporous polystyrene and carbon materials with core-shell nanosphere-interconnected network structure. *Macromolecules* **44**, 5846–5849 (2011).
38. Wu, D. C. *et al.* Preparation of polymeric nanoscale networks from cylindrical molecular bottlebrushes. *ACS Nano* **6**, 6208–6214 (2012).
39. Wu, D. C. *et al.* Design and preparation of porous polymers. *Chem. Rev.* **112**, 3959–4015 (2012).
40. Jagiello, J. & Olivier, J. P. A simple two-dimensional NLDFT model of gas adsorption in finite carbon pores. application to pore structure analysis. *J. Phys. Chem. C* **113**, 19382–19385 (2009).
41. Ravikovitch, P. I., Vishnyakov, A., Russo, R. & Neimark, A. V. Unified approach to pore size characterization of microporous carbonaceous materials from N_2, Ar, and CO_2 adsorption isotherms. *Langmuir* **16**, 2311–2320 (2000).
42. Huang, H. Y. *et al.* Solvent-induced morphological transition in core-cross-linked block copolymer micelles. *J Am Chem Soc* **128**, 3784–3788 (2006).
43. Peng, B., van der Wee, E., Imhof, A. & van Blaaderen, A. Synthesis of monodisperse, highly cross-linked, fluorescent PMMA particles by dispersion polymerization. *Langmuir* **28**, 6776–6785 (2012).
44. Panyam, J. & Labhasetwar, V. Biodegradable nanoparticles for drug and gene delivery to cells and tissue. *Adv. Drug Deliv. Rev.* **55**, 329–347 (2003).
45. Acharya, G. & Park, K. Mechanisms of controlled drug release from drug-eluting stents. *Adv. Drug Deliv. Rev* **58**, 387–401 (2006).
46. Liu, C., Li, F., Ma, L. P. & Cheng, H. M. Advanced materials for energy storage. *Adv. Mater.* **22**, E28–E62 (2010).
47. Su, D. S. & Schlögl, R. Nanostructured carbon and carbon nanocomposites for electrochemical energy storage applications. *Chemsuschem* **3**, 136–168 (2010).
48. Wang, Y. *et al.* A facile soft-template synthesis of ordered mesoporous carbon/tungsten carbide composites with high surface area for methanol electrooxidation. *J. Power Sources* **200**, 8–13 (2012).
49. Noked, M., Soffer, A. & Aurbach, D. The electrochemistry of activated carbonaceous materials: past, present, and future. *J. Solid State Electr.* **15**, 1563–1578 (2011).
50. Inagaki, M., Yang, Y. & Kang, F. Y. Carbon nanofibers prepared via electrospinning. *Adv. Mater.* **24**, 2547–2566 (2012).
51. Zhang, W. F. *et al.* Porous carbon for electrochemical capacitors prepared from a resorcinol/formaldehyde-based organic aquagel with nano-sized particles. *J. Mater. Chem.* **22**, 7158–7163 (2012).
52. Wu, D. C. *et al.* Novel nanoporous carbons from well-defined poly(styrene-co-acrylonitrile)-grafted silica nanoparticles. *Chem. Mater.* **23**, 2024–2026 (2011).
53. Tang, C. *et al.* Nanoporous carbon films from "hairy" polyacrylonitrile-grafted colloidal silica nanoparticles. *Adv. Mater.* **20**, 1516–1522 (2008).
54. Yang, X. Q., Wu, D. C. & Fu, R. W. Nanoporous carbon produced from a styrene-acrylonitrile random copolymer/carbon nanotube composite. *Micro. Nano Lett.* **5**, 105–109 (2010).
55. Li, G. B. *et al.* Raman scattering investigation of carbons obtained by heat treatment of a polyfurfuryl alcohol. *Solid State Ionics* **89**, 327–331 (1996).
56. Baratta, G. A. *et al.* Raman spectroscopy of ion irradiated amorphous carbons. *Nucl. Instrum. Methods Phys. Res. Sect. B* **116**, 195–199 (1996).
57. Ungar, T., Gubicza, J., Ribarik, G., Pantea, C. & Zerda, T. W. Microstructure of carbon blacks determined by X-ray diffraction profile analysis. *Carbon* **40**, 929–937 (2002).
58. Jawhari, T., Roid, A. & Casado, J. Raman spectroscopic characterization of some commercially available carbon black materials. *Carbon* **33**, 1561–1565 (1995).
59. Song, J. S., Tronc, F. & Winnik, M. A. Two-stage dispersion polymerization toward monodisperse, controlled micrometer-sized copolymer particles. *J. Am. Chem. Soc.* **126**, 6562–6563 (2004).

Acknowledgement

This research was supported by the project of NNSFC (51173213, 50802116, 51172290, 51232005), Program for New Century Excellent Talents in University (NCET-12-0572), Program for Pearl River New Star of Science and Technology in Guangzhou, and the Fundamental Research Funds for the Central Universities (13lgpy57, 09lgpy18).

Author contributions

D.W. conceived the project. Y.O. and H.S. conducted the experiments. D.W., Y.O., H.S. and R.F. discussed the results. D.W. and Y.O. wrote the manuscript.

Additional information

Supplementary information accompanies this paper at http://www.nature.com/scientificreports

Competing financial interests: The authors declare no competing financial interests.

How to cite this article: Ouyang, Y., Shi, H., Fu, R. & Wu, D. Highly Monodisperse Microporous Polymeric and Carbonaceous Nanospheres with Multifunctional Properties. *Sci. Rep.* **3**, 1430; DOI:10.1038/srep01430 (2013).